

# 2'-Fluoro RNA Shows Increased Watson–Crick H-Bonding Strength and Stacking Relative to RNA: Evidence from NMR and Thermodynamic Data\*\*

Amritraj Patra, Michael Paolillo, Klaus Charisse, Muthiah Manoharan, Eriks Rozners,\* and Martin Egli\*

Oligonucleotides containing 2'-deoxy-2'-fluororibonucleotides (2'-F RNA) have found numerous beneficial applications in ribozyme-,<sup>[1]</sup> antisense-,<sup>[2,3]</sup> siRNA-,<sup>[4,5]</sup> miRNA-,<sup>[6]</sup> and aptamer-based<sup>[7]</sup> nucleic acid therapeutics. Moreover, antisense oligonucleotides bearing 2'-F ribonucleotides were recently found to exhibit favorable properties for modulating splicing, relative to other 2'-modifications.<sup>[8]</sup> At the 2'-position of the ribose ring, fluorine preorganizes the sugar in a C3'-endo conformation that matches the preferred structure of RNA duplexes. We found that siRNAs extensively modified with 2'-F pyrimidines showed increased nuclease stability, reduced immune stimulation, and in some cases exhibited favorable activity in vitro and in vivo, relative to unmodified control RNA.<sup>[5]</sup> The stabilizing effect of 2'-F modification, as measured by the thermal melting temperature of RNA duplexes, amounts to approximately 1.8 °C per nucleotide.

Comparison of the crystal structures of all-RNA, all-2'-F RNA, and mixed-RNA/2'-F RNA octamer duplexes revealed that substitution of the 2'-OH by 2'-F has very little effect on the local and overall helix geometry.<sup>[9]</sup> Owing to the atomic resolution of the diffraction data, and in combination with osmotic-stress data, our study also established differences in the hydration patterns of 2'-F RNA and RNA. 2'-F is a poor H-bond acceptor in the minor groove,<sup>[9]</sup> whereas 2'-OH is extensively hydrated and serves as a bridge head for water molecules linking strands across the minor groove.<sup>[5,9,10]</sup>

Unexpectedly, given the poor hydration of 2'-F and the general assumption that fluorine preorganizes the backbone for the RNA target, thermodynamic data indicated that the higher stability of 2'-F RNA is entirely based on favorable enthalpy and not entropy.<sup>[9]</sup>

Base stacking and H-bonding are the main contributors to the enthalpic change as a result of duplex formation. However, it is not immediately clear if only one of these factors accounts for the stability increase or whether both contribute. To gain a better understanding of the source(s) of the favorable enthalpy of duplex formation displayed by 2'-F RNA, we conducted a series of NMR and thermodynamic experiments.

H-bond lengths can be empirically determined by measuring the one-bond scalar coupling ( $^1J_{\text{NH}}$ )<sup>[11]</sup> of Watson–Crick C:G and A:U base-pairs and by tracing the proton chemical shifts  $\delta(^1\text{H})$  of imino protons.<sup>[12,13]</sup> Grzesiek and co-workers showed that with decreasing H-bond distance (increasing strength),  $\delta(^1\text{H})$  increases, whereas  $^1J_{\text{NH}}$  becomes less negative in DNA.<sup>[14]</sup> LiWang and co-workers measured  $^1J_{\text{NH}}$  coupling constants at natural abundance  $^{15}\text{N}$  to demonstrate that N1...H–N3 hydrogen bonds in RNA A:U base-pairs are stronger than those in DNA A:T base-pairs.<sup>[15]</sup> The comparison of the H-bonding strengths in DNA and RNA duplexes may be complicated by the presence of the 5-methyl group on the T residue compared to a U residue,<sup>[16]</sup> as well as the different stacking types (intrastrand in DNA and interstrand in RNA).<sup>[17]</sup> By comparison, the virtually identical conformations of RNA and 2'-F RNA duplexes<sup>[9]</sup> pose no problems in this respect.

We used two oligonucleotides, 2'-F RNA 5'-I(CGAAUUCG)-3' and RNA 5'-r(CGAAUUCG)-3' at natural abundance  $^{15}\text{N}$  to assess a potential effect on  $^1J_{\text{NH}}$  for  $^{15}\text{N}$ - $^1\text{H}$  imino groups in C:G and A:U base-pairs as a result of replacing the 2'-hydroxy group with fluorine (Figure 1). Individual proton resonances were assigned using a combination of NOESY, DQF-COSY, and TOCSY spectra and conventional assignment strategies for double stranded RNA (Supporting Information, Figure S2). The  $^1\text{H}$  NMR spectra in 10%  $\text{D}_2\text{O}/\text{H}_2\text{O}$  showed all four imino resonances, confirming the double-helical structures (Figure 2).  $^1J_{\text{NH}}$  coupling constants for imino groups were measured following published methods and by adapting the two-dimensional in-phase anti phase (IPAP) technique to an  $^{15}\text{N}$ -filtered, 1D proton-detected, one-dimensional NMR measurement.<sup>[15]</sup> The  $^1J_{\text{NH}}$  coupling values for imino groups from the three internal base-pairs are depicted in Figure 1. As expected we

[\*] Dr. A. Patra, Prof. M. Egli  
Department of Biochemistry,  
Vanderbilt University School of Medicine  
Nashville, TN 37232-0146 (USA)  
E-mail: martin.egli@vanderbilt.edu  
Homepage: <http://structbio.vanderbilt.edu/~eglim/>

M. Paolillo, Prof. E. Rozners  
Department of Chemistry,  
State University of New York at Binghamton  
Binghamton, NY 13902 (USA)  
erozners@binghamton.edu

Dr. K. Charisse, Dr. M. Manoharan  
Alnylam Pharmaceuticals  
300 Third Street, Cambridge, MA 02142 (USA)

[\*\*] Supported by NIH grants R01 GM055237 (M.E.) and R01 GM071461 (E.R.). We thank Dr. Markus Voehler and Dr. Min-Kyu Cho for help with NMR acquisition, Raquel Rozner and Ryan Merrihue for assistance with UV melting experiments, and Prof. Nicholas Reiter for helpful discussions.

Supporting information for this article (experimental details) is available on the WWW under <http://dx.doi.org/10.1002/anie.201204946>.

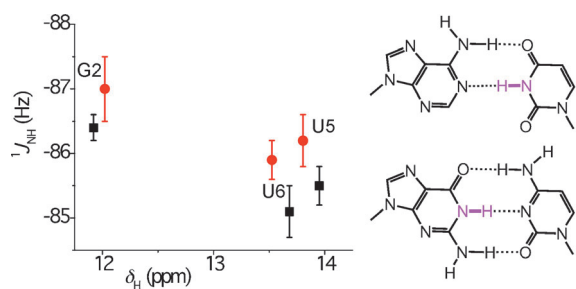


**Figure 1.** Chemical shifts of imino protons  $\delta_{\text{H}}$  (highlighted in magenta in the A:U and G:C base-pair diagrams) versus one-bond scalar coupling constants  $J_{\text{NH}}$ , for 2'-F RNA (black squares) and RNA (red dots) of sequence  $\text{C}_1\text{G}_2\text{A}_3\text{A}_4\text{U}_5\text{U}_6\text{C}_7\text{G}_8$ . The graph shows average values with standard deviations (vertical bars) based on six independent one-dimensional  $^{15}\text{N}$ -coupled  $^1\text{H}$  IPAP spectra of the imino region in 10%  $\text{D}_2\text{O}/\text{H}_2\text{O}$  at 5°C (note the reversed scale on the y-axis). Entries around 12 ppm are for the G2 base, and those at 13.5 and 14 ppm are for the U6 and U5 bases, respectively. The average difference in  $J_{\text{NH}}$  between 2'-F RNA and RNA amounts to  $0.8 \pm 0.3$ .

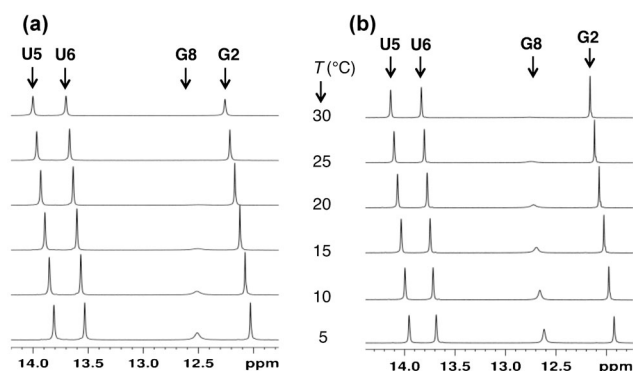


**Figure 2.** Overlay of one-dimensional proton spectra of the imino region for a) 5'-r(CGAAUUCG)-3' and b) 5'-f(CGAAUUCG)-3' in 10%  $\text{D}_2\text{O}/\text{H}_2\text{O}$ . The spectra were recorded at varying temperatures, from 5°C to 30°C. Protons shown are assigned as U5, U6, G8 and G2 in the two duplexes.

could not measure the  $J_{\text{NH}}$  values for terminal C:G base pairs due to rapid exchange with solvent.

The plot of chemical shifts for RNA and 2'-F RNA versus the corresponding  $J_{\text{NH}}$  couplings shows that 2'-F RNA  $J_{\text{NH}}$  values are less negative than those in RNA by an average of  $0.8 \pm 0.3$ . The chemical shifts of three of the four imino protons in 2'-F RNA increase compared to RNA (Figure 2 and Supporting Information), thus indicating increased H-bonding strength. In line with this interpretation, we found that the terminal C:G base-pairs in 2'-F RNA tend to be more strongly paired than in native RNA, arguably due to stronger H-bonding, as measured by line broadening of the G8 imino proton at specific temperatures (Figure 2). The direction and magnitude of the changes in the  $J_{\text{NH}}$  couplings and/or chemical shifts  $\delta(^1\text{H})$  in 2'-F RNA relative to RNA are also consistent with the previously established changes in these parameters between RNA and DNA.<sup>[15]</sup> The stronger electro-

negativity of the 2'-fluoro substituent, compared to 2'-OH, can reasonably be expected to further polarize nucleobase functions.

To corroborate the observed differences in H-bonding between 2'-F RNA and RNA based on  $J_{\text{NH}}$  coupling and temperature-dependent line widths, we measured the deuterium isotope effect (DIE) on the C2 atom of adenine in A:U base-pairs (see inset in Figure 1) as a result of H/D exchange at the N3 atom of uracil.<sup>[18,19]</sup> As a consequence of the slow N3(U) imino hydrogen exchange with solvent, the  $^{13}\text{C}$  resonances from adenine split into doublets, whereby the magnitude of the splitting provides a measure of the strength of the H-bond. Accordingly, larger absolute values in the difference in chemical shift ( $^2\text{h}\Delta^{13}\text{C}2$  in parts per billion, ppb) are indicative of increased H-bonding strength. To quantify the DIE we acquired  $^1\text{H}$ ,  $^{13}\text{C}$  HMQC spectra for the 2'-F RNA and RNA octamers (Figure 3). Consistent with earlier measurements for RNA<sup>[18]</sup> we found an average value for  $^2\text{h}\Delta^{13}\text{C}2$  of  $-56.7$  ppb for A3 and A4 in r(CGAAUUCG). By comparison, the average value for  $^2\text{h}\Delta^{13}\text{C}2$  for the corresponding residues in f(CGAAUUCG) was  $-63.2$  ppb (see Table S1 in the Supporting Information for individual values). Thus, the DIE data support the above observations of increased Watson–Crick H-bonding strength in 2'-F RNA relative to RNA.

To assess a potential contribution of base stacking to the stabilization of 2'-F RNA relative to RNA, we studied the thermodynamics of short hairpins,<sup>[20]</sup> either with blunt ends or 3'-overhanging nucleotides (Figure 4a). Because the overhanging nucleotide(s) cannot form interstrand hydrogen bonds, this is a well-established model system to measure differences in base stacking.<sup>[21–23]</sup> Because of the negative inclination of the RNA backbone relative to the base-pair axes, a 3'-dangling purine stacking onto the 5'-terminal purine from the opposite strand typically results in a considerably higher stabilization than a 5'-dangling residue or either 3'- or 5'-dangling ends in duplex DNA.<sup>[21,24]</sup> Indeed, addition of a single adenosine at the 3'-end of the 5'-GCGUUUUCGC hairpins led to significant increases in the thermodynamic stability (Table 1, sequences 1 versus 2 and 4 versus 5). The melting temperature of the hairpin was increased by almost

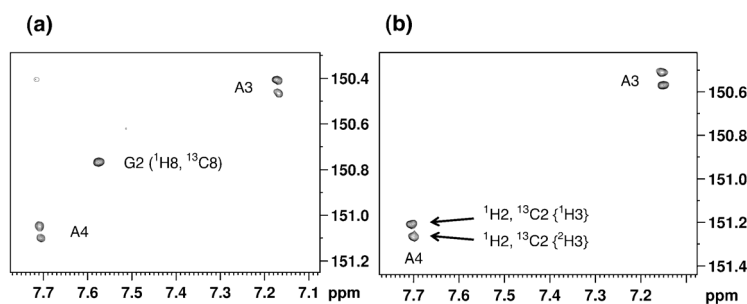


**Figure 3.** Region of  $^1\text{H}$ ,  $^{13}\text{C}$  HMQC spectra of a) 5'-r(CGAAUUCG)-3' and b) 5'-f(CGAAUUCG)-3', showing the isotope effect at  $^{13}\text{C}2$  of adenosine residues owing to deuterium/proton substitution at the imino H3 site. The individual spectra were recorded at natural abundance  $^{13}\text{C}$  in 50%  $\text{D}_2\text{O}/\text{H}_2\text{O}$  at 25°C at 14.1 T (600 MHz  $^1\text{H}$  frequency). The x-axis shows  $^1\text{H}$  nuclei and the y-axis shows  $^{13}\text{C}$  nuclei. The DIE measurements ( $^2\text{h}\Delta^{13}\text{C}2 = \delta^{13}\text{C}2\{^1\text{H}3\} - \delta^{13}\text{C}2\{^2\text{H}3\}$ ) show that 2'-F RNA exhibits a larger isotope effect than RNA (see Supporting Information, Table S1).

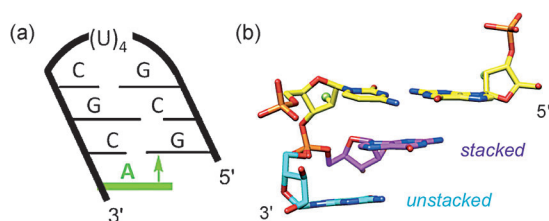


**Figure 4.** a) Hairpin construct used to assess the contribution of base stacking to the relative stabilities of 2'-F RNA and RNA. The negative inclination between backbone and base pairs in 2'-F RNA and RNA results in considerable cross-strand stacking<sup>[23,24]</sup> and a stabilizing  $\pi$ - $\pi$  interaction (arrow) between the 3'-overhanging A residue (green) and the 5'-terminal G residue. b) Dual conformations of a 3'-terminal G residue in the crystal structure of a mixed 2'-F/2'-OH RNA duplex (PDB ID: 3P4C),<sup>[9]</sup> unstacked (cyan carbons) and stacked (magenta carbons) onto the terminal C:G pair (yellow carbons). F2' atoms of the terminal pair are green spheres. Neither conformation of the G residue features an intranucleoside H-bond involving the 2'-OH moiety.

17°C by addition of a 2'-fluoro-A (terminal fC:fG pair) compared to an increase of 11.6°C by addition of a 2'-ribo-A (terminal rC:rG pair). Van't Hoff analysis of the UV melting curves (Table 1, columns 4–6) showed that the stabilization was driven by an enhanced binding enthalpy and was larger for 2'-F RNA ( $\Delta\Delta G = 2.2$ ,  $\Delta\Delta H = 8.7$  kcal mol<sup>-1</sup>) than for RNA ( $\Delta\Delta G = 1.4$ ,  $\Delta\Delta H = 4.3$  kcal mol<sup>-1</sup>). The larger  $\Delta\Delta H$  for the 2'-F RNA relative to RNA overhangs indicates that at least a part of the enthalpic stabilization of 2'-F RNA is due to enhanced base stacking. The effect of the addition of a second overhanging adenosine was relatively small by comparison and the difference between 2'-F RNA and RNA was within the error limits of the data. The enthalpy calculated using differentiated melting curves<sup>[25]</sup> (see Supporting Information for experimental details) showed a similar trend (Table 1, column 3).

Using osmotic stress experiments<sup>[26–28]</sup> (Table 1, columns 7 and 8), we determined that the blunt hairpins (sequences 1 and 4) were poorly hydrated, presumably because the short stem and the relatively flexible uridine tetraloop did not provide good enough anchors for a stable hydration network.

The NMR solution structure of an RNA hairpin with a U<sub>4</sub> loop revealed an absence of hydrogen bonding and stacking interactions among the uracil residues<sup>[29,30]</sup> (Supporting Information, Figure S11). These conformational properties are consistent with the reduced thermodynamic stability of the U<sub>4</sub> loop compared with the more common UUCG and GNRA (N = any nucleotide; R = purine) RNA tetraloops that both feature intricate interactions among loop residues.<sup>[31]</sup> Addition of one adenosine residue caused a significant increase in hydration of the hairpins. Consistent with our previous findings that the 2'-F modification caused dehydration of duplex RNA,<sup>[9]</sup> the increase of hydration upon addition of one adenosine appeared to be somewhat smaller for 2'-F RNA than for RNA, although the differences were within the limits of experimental error. Therefore, the differential stabilizations afforded by 3'-dangling 2'-F and 2'-OH adenosine residues cannot be attributed to hydration. Similarly, it is unlikely that conformational differences between the 2'-F and 2'-OH adenosine residues (that is, owing to an intranucleoside O2'-H...N3 hydrogen bond that is absent in the 2'-F nucleoside) affect the respective gains in stacking enthalpy in a crucial way. Thus, we did not observe formation of such an H-bond in the unstacked configuration of a 3'-terminal G residue with dual occupancy in the crystal structure of a mixed 2'-F/2'-OH RNA duplex (Figure 4b).<sup>[9]</sup>

The combined NMR spectroscopic and thermodynamic data provide evidence that electronic effects of the 2'-fluorine substituent in the axial configuration boost the RNA affinity of the modified strand by favorably affecting both Watson-Crick H-bonding and base stacking. The gains in H-bonding are consistent with less negative <sup>1</sup>J<sub>NH</sub> couplings (N3H of both U residues and N1H of G2), increased chemical shifts (imino protons of both U residues and G8), and reduced line widths, in particular for N1H of terminal G8, in 2'-F RNA relative to RNA. Our observations are also consistent with those of others who had used a similar strategy based on measurements of <sup>1</sup>J<sub>NH</sub> coupling constants to establish the increased strength of [A]N1...H-N3[U/T] H-bonds in duplex RNA relative to duplex DNA.<sup>[15]</sup> Thus, it appears that the more electronegative fluorine polarizes imino moieties more strongly than the RNA 2'-hydroxy group, thereby tightening

**Table 1:** Thermodynamic data for RNA and 2'-F modified RNA hairpins with or without 3'-terminal A or 2'-F A overhangs.<sup>[a]</sup>

Hairpin sequence <sup>[b]</sup>	<i>T<sub>m</sub></i> [°C]	$\Delta T_m^{[c]}$	$-\Delta H$ $\delta a/\delta T_m$ [kcal mol <sup>-1</sup> ]	$\Delta\Delta H^{[c]}$	$-\Delta H$ Van't Hoff [kcal mol <sup>-1</sup> ]	$\Delta\Delta H^{[c]}$	$-\Delta S$ Van't Hoff [cal mol <sup>-1</sup> K]	$-\Delta G$ (at 37 °C) [kcal mol <sup>-1</sup> ]	$\Delta\Delta G^{[c]}$	$\Delta n_w^{[d]}$ ethylene glycol	$\Delta\Delta n_w^{[c]}$	$\Delta n_w^{[d]}$ acetamide	$\Delta\Delta n_w^{[c]}$
1. GCGUUUUCGC	51.9 ± 0.6		27.8 ± 0.6		30.9 ± 0.8		95.0 ± 2.6	1.5 ± 0.1		9 ± 3		16 ± 2	
2. GCGUUUUCGCA	63.5 ± 0.4	<b>11.6</b>	34.2 ± 1.3	<b>6.4</b>	35.2 ± 1.6	<b>4.3</b>	104.3 ± 4.6	2.9 ± 0.2	<b>1.4</b>	23 ± 3	<b>14</b>	29 ± 3	<b>13</b>
3. GCGUUUUCGCAA	67.9 ± 0.4	<b>4.4</b>	35.7 ± 1.7	<b>1.5</b>	38.2 ± 2.7	<b>3.0</b>	112.1 ± 7.7	3.5 ± 0.3	<b>0.6</b>	20 ± 2	<b>-3</b>	34 ± 3	<b>5</b>
4. GfCGUUUUCGcf	57.4 ± 0.3		26.5 ± 1.4		29.5 ± 1.4		89.0 ± 4.5	1.9 ± 0.1		8 ± 2		15 ± 2	
5. GfCGUUUUCGC-fAf	74.3 ± 0.5	<b>16.9</b>	36.0 ± 3.0	<b>9.5</b>	38.2 ± 1.2	<b>8.7</b>	110.1 ± 3.6	4.1 ± 0.1	<b>2.2</b>	18 ± 4	<b>10</b>	27 ± 4	<b>12</b>
6. GfCGUUUUCGC-fAfAf	77.1 ± 0.3	<b>2.8</b>	36.3 ± 1.0	<b>0.3</b>	39.2 ± 1.3	<b>1.0</b>	111.8 ± 3.8	4.5 ± 0.2	<b>0.4</b>	21 ± 3	<b>3</b>	28 ± 3	<b>1</b>

[a] Melting of each oligonucleotide hairpin (16 μM) was performed in 10 mM sodium cacodylate (pH 7.4), 0.1 mM EDTA, and 300 mM NaCl. [b] Loop residues are underlined, Cf, Gf, and Af indicate 2'-F modified C, G, and A, respectively, and 3'-overhanging A or Af nucleotides are highlighted in bold font. [c] Differences in *T<sub>m</sub>*,  $\Delta H$ ,  $\Delta G$ , or  $\Delta n_w$  ( $\Delta\Delta$  values) between a blunt-end hairpin (1 and 4) and a hairpin with a single overhang (2 and 5) are shown as the first value in bold, or a hairpin with a single overhang (2 and 5) and two overhangs (3 and 6) are shown as the second value in bold.

[d]  $\Delta n_w$  = number of water molecules released upon melting.

Watson–Crick H-bonds and contributing to the previously established, favorable  $\Delta H$  term underlying the higher RNA affinity of 2'-F RNA relative to RNA.<sup>[9]</sup>

Whereas an investigation of the role of the 2'-hydroxy group in potentially strengthening base stacking interactions in A-form RNA relative to B-form DNA duplexes is complicated by different stacking types in the two species,<sup>[17,23,24]</sup> the A-form conformation of 2'-F RNA and RNA<sup>[9]</sup> allows for a direct comparison. The thermodynamic data gathered for native and 2'-F modified RNA hairpins with A residue overhangs support a favorable effect of fluorine on stacking. Given the long reach of fluorine in terms of the aforementioned polarization of imino protons, the effect on the entire aromatic system is not surprising. Fluorine directly attached to the base (that is, in the T analogue 2,4-difluorotoluene) resulted in increased stacking interactions in DNA duplexes as assessed by dangling ends.<sup>[22]</sup> Moreover NMR experiments provided evidence that Watson–Crick H-bonding and stacking interactions are coupled in DNA.<sup>[32]</sup>

In summary, the higher, enthalpy-based stability of 2'-F RNA relative to RNA is the result of a strengthening of both the H-bonding and stacking interactions in the modified duplex. Our findings provide evidence that the electron-withdrawing power of fluorine in an antiperiplanar orientation to the glycosidic bond is propagated through the entire nucleobase moiety and that such effects dominate a potential role of fluorine in the higher rigidity of the 2'-F RNA backbone compared with RNA. The results described herein are directly relevant in terms of the origins of the higher stabilities of mimics of 2'-F RNA, 3'-fluoro hexitol nucleic acid (F-HNA)<sup>[3]</sup> and 3'-fluoro cyclohexenyl nucleic acid (F-CeNA),<sup>[33]</sup> relative to HNA and CeNA, respectively.

Received: June 25, 2012

Revised: August 21, 2012

Published online: October 10, 2012

**Keywords:** 2'-F RNA · hydrogen bonding · NMR spectroscopy · RNA · thermodynamics

- [1] W. A. Pieken, D. B. Olsen, F. Benseler, H. Aurup, F. Eckstein, *Science* **1991**, 253, 314–317.
- [2] A. M. Kawasaki, M. D. Casper, S. M. Freier, E. A. Lesnik, M. C. Zounes, L. L. Cummins, C. Gonzalez, P. Dan Cook, *J. Med. Chem.* **1993**, 36, 831–841.
- [3] M. Egli, P. S. Pallan, C. Allerson, T. Prakash, A. Berdeja, J. Yu, S. Lee, A. Watt, H. Gaus, B. Bhat, E. Swayze, P. Seth, *J. Am. Chem. Soc.* **2011**, 133, 16442–16449.
- [4] C. R. Allerson, N. Sioufi, R. Jarres, T. P. Prakash, N. Naik, A. Berdeja, L. Wanders, R. H. Griffey, E. E. Swayze, B. Bhat, *J. Med. Chem.* **2005**, 48, 901–904.
- [5] M. Manoharan, A. Akinc, R. K. Pandey, J. Qin, P. Hadwiger, M. John, K. Mills, K. Charisse, M. A. Maier, L. Nechev, E. M. Greene, P. S. Pallan, E. Rozners, K. G. Rajeev, M. Egli, *Angew. Chem.* **2011**, 123, 2332–2336; *Angew. Chem. Int. Ed.* **2011**, 50, 2284–2288.

- [6] S. Davis, S. Propp, S. M. Freier, L. E. Jones, M. J. Serra, G. Kinberger, B. Bhat, E. E. Swayze, C. F. Bennett, C. Esau, *Nucleic Acids Res.* **2009**, 37, 70–77.
- [7] E. W. M. Ng, D. T. Shima, P. Calias, E. T. Cunningham, D. R. Guyer, A. P. Adamis, *Nat. Rev. Drug Discovery* **2006**, 5, 123–132.
- [8] F. Rigo, Y. Hua, S. J. Chun, T. P. Prakash, A. R. Krainer, F. Bennett, *Nat. Chem. Biol.* **2012**, 8, 555–561.
- [9] P. S. Pallan, E. M. Greene, P. A. Jicman, R. K. Pandey, M. Manoharan, E. Rozners, M. Egli, *Nucleic Acids Res.* **2011**, 39, 3482–3495.
- [10] M. Egli, S. Portmann, N. Usman, *Biochemistry* **1996**, 35, 8489–8494.
- [11] A. J. Dingley, J. E. Masse, R. D. Peterson, M. Barfield, J. Feigon, S. Grzesiek, *J. Am. Chem. Soc.* **1999**, 121, 6019–6027.
- [12] S. S. Wijmenga, M. Kruithof, C. W. Hilbers, *J. Biomol. NMR* **1997**, 10, 337–350.
- [13] J. Czernek, R. Fiala, V. Sklenar, *J. Magn. Reson.* **2000**, 145, 142–146.
- [14] M. Barfield, A. J. Dingley, J. Feigon, S. Grzesiek, *J. Am. Chem. Soc.* **2001**, 123, 4014–4022.
- [15] M. N. Manalo, X. Kong, A. LiWang, *J. Am. Chem. Soc.* **2005**, 127, 17974–17975.
- [16] M. Swart, C. F. Guerra, F. M. Bickelhaupt, *J. Am. Chem. Soc.* **2004**, 126, 16718–16719.
- [17] M. Egli in *Nucleic Acids in Chemistry and Biology*, 3<sup>rd</sup> ed. (Eds.: G. M. Blackburn, M. J. Gait, D. Loakes, D. M. Williams), Royal Society of Chemistry, Cambridge, UK, **2006**, pp. 13–75.
- [18] I. Vakonakis, A. C. LiWang, *J. Am. Chem. Soc.* **2004**, 126, 5688–5689.
- [19] I. Vakonakis, A. C. LiWang, *J. Biomol. NMR* **2004**, 29, 65–72.
- [20] B. Reif, V. Wittmann, H. Schwalbe, C. Griesinger, K. Wörner, K. Jahn-Hofmann, J. W. Engels, W. Bermel, *Helv. Chim. Acta* **1997**, 80, 1952–1971.
- [21] S. M. Freier, R. Kierzek, J. A. Jaeger, N. Sugimoto, M. H. Caruthers, T. Neilson, D. H. Turner, *Proc. Natl. Acad. Sci. USA* **1986**, 83, 9373–9377.
- [22] K. Guckian, B. A. Schweitzer, R. X.-F. Ren, C. J. Sheils, P. L. Paris, D. C. Tahmassebi, E. T. Kool, *J. Am. Chem. Soc.* **1996**, 118, 8182–8183.
- [23] R. Micura, M. Bolli, N. Windhab, A. Eschenmoser, *Angew. Chem.* **1997**, 109, 899–902; *Angew. Chem. Int. Ed. Engl.* **1997**, 36, 870–873.
- [24] P. S. Pallan, P. Lubini, M. Bolli, M. Egli, *Nucleic Acids Res.* **2007**, 35, 6611–6624.
- [25] K. J. Breslauer, *Methods Enzymol.* **1995**, 259, 221–242.
- [26] C. H. Spink, J. B. Chaires, *Biochemistry* **1999**, 38, 496–508.
- [27] E. Rozners, J. Moulder, *Nucleic Acids Res.* **2004**, 32, 248–254.
- [28] E. Rozners, *Curr. Protoc. Nucleic Acid Chem.* **2010**, 43, 7.14.1–7.14.13.
- [29] P. L. Vanegas, G. A. Hudson, A. R. Davis, S. C. Kelly, C. C. Kirkpatrick, B. M. Znosko, *Nucleic Acids Res.* **2012**, 40, D439–D444; <http://cosmos.slu.edu>.
- [30] D. G. Sashital, V. Venditti, C. G. Angers, G. Cornilescu, S. E. Butcher, *RNA* **2007**, 13, 328–338.
- [31] J. P. Sheehy, A. R. Davis, B. M. Znosko, *RNA* **2010**, 16, 417–429.
- [32] M. N. Manalo, L. M. Pérez, A. LiWang, *J. Am. Chem. Soc.* **2007**, 129, 11298–11299.
- [33] P. P. Seth, J. Yu, A. Jazayeri, P. S. Pallan, C. R. Allerson, M. E. Østergaard, F. Liu, P. Herdewijn, M. Egli, E. E. Swayze, *J. Org. Chem.* **2012**, 77, 5074–5085.

## **Supporting Information**

### **Contents**

1. NMR experiments	Page S2
2. Figure S1: One dimensional $^1\text{H}$ NMR spectra	S3
3. Figure S2: Expanded NOESY spectra	S4
4. Figure S3: Low field regions of $^1\text{H}$ -NMR spectra	S6
5. Figure S4: IPAP spectra	S7
6. Deuterium isotope effect measurements, Table S1	S8
7. UV thermal melting experiments	S9
8. UV melting and osmotic stress data for RNA and 2'-F RNA hairpins, Tables S2 to S7 and Figures S5 to S10	S10
9. Figure S11: NMR solution structure of RNA hairpin with U <sub>4</sub> loop	S22

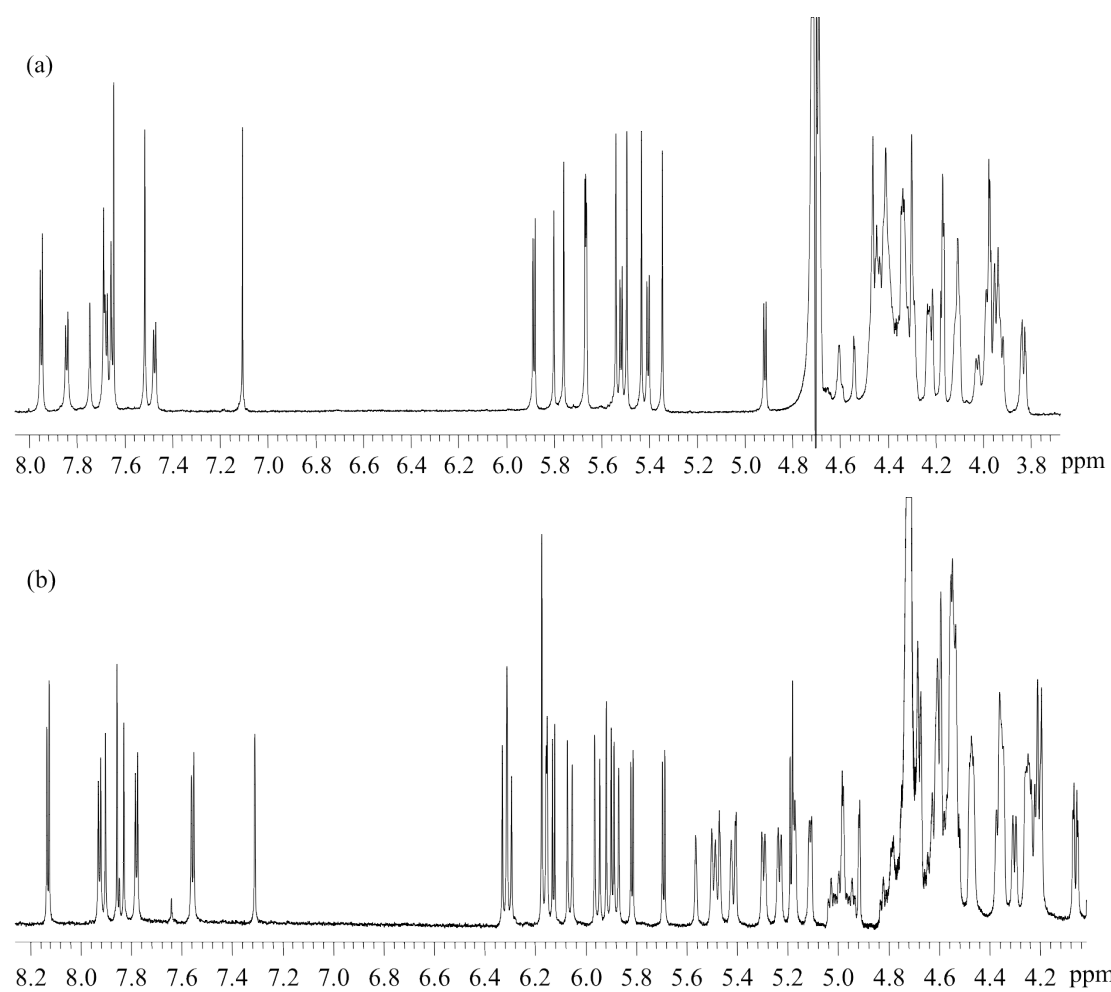
## 1. NMR experiments

Oligonucleotides were purified by RP-HPLC using a TEAA/acetonitrile buffer mixture and were lyophilized several times from aqueous ammonium solution and water to remove any trace of volatile HPLC material prior to preparation of the NMR sample. Oligonucleotides were dissolved in 180  $\mu$ L of D<sub>2</sub>O containing 150 mM NaCl and 10 mM phosphate buffer (Na<sub>2</sub>HPO<sub>4</sub>/KH<sub>2</sub>PO<sub>4</sub>) at pH 7.4 (uncorrected for deuterium effect) for NMR analysis. The concentration of the 2'-F RNA sample was 1.4 mM and that of the native RNA was 1.75 mM. For the acquisition of spectra containing the exchangeable protons, the sample was dried and the residue immediately taken up in 180  $\mu$ L of H<sub>2</sub>O/D<sub>2</sub>O (9:1; v/v).

NMR experiments were performed either on Bruker AVANCE 800 MHz or 600 MHz spectrometers. Different sets of two-dimensional spectra were recorded at different temperatures varying from 5 to 40°C. NOESY experiments in D<sub>2</sub>O buffer were acquired with mixing times of 400, 250, 125, and 62.5 ms. NOESY spectra detecting exchangeable protons were recorded with mixing times of 400, 250, and 100 ms. DQF-COSY and TOCSY spectra were recorded to aid the assignment, the latter with a mixing time of 80 ms. All two-dimensional spectra were acquired with 2k complex data points in *t*<sub>2</sub> and 512 real points in *t*<sub>1</sub> with a relaxation delay of 2 s.

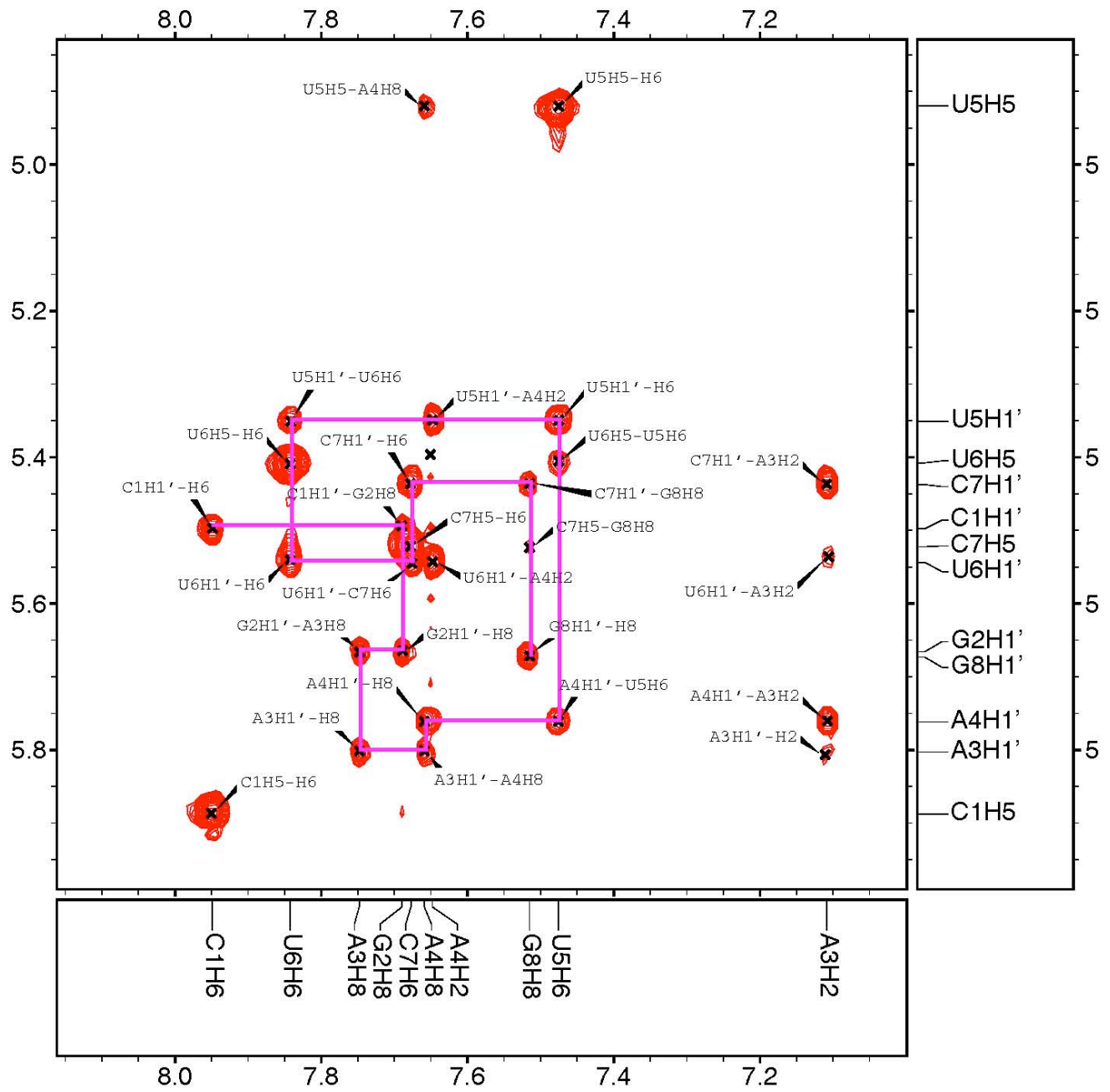
<sup>1</sup>H, <sup>13</sup>C HMQC spectra were recorded on a Bruker AVANCE 14.1 T (600 MHz, <sup>1</sup>H nuclei) spectrometer at 25°C in 50% D<sub>2</sub>O/H<sub>2</sub>O. Two-dimensional spectra were acquired with 2k complex data points in *t*<sub>2</sub> and 128 real points in *t*<sub>1</sub> with a relaxation delay of either 2 s or 1.5 s.

Sequential assignment of exchangeable and non-exchangeable protons was conducted following standard methods for duplex RNA. The DQF-COSY spectrum showed four pairs of cross peaks, characteristic of J-coupled spins of the H<sub>5</sub> and H<sub>6</sub> protons in cytosine and uracil rings. Due to their labile nature H<sub>8</sub> protons from guanine bases in 2'-F RNA were difficult to assign and were therefore identified from leftover cross peaks and from H<sub>8</sub>/H<sub>2'</sub> cross peaks.



**Figure S1.** One dimensional  $^1\text{H}$  NMR spectrum of (a)  $[\text{r}(\text{CGAAUUCG})]_2$  and (b)  $[\text{f}(\text{CGAAUUCG})]_2$  in phosphate-buffered  $\text{D}_2\text{O}$  at  $25^\circ\text{C}$ .

(a)



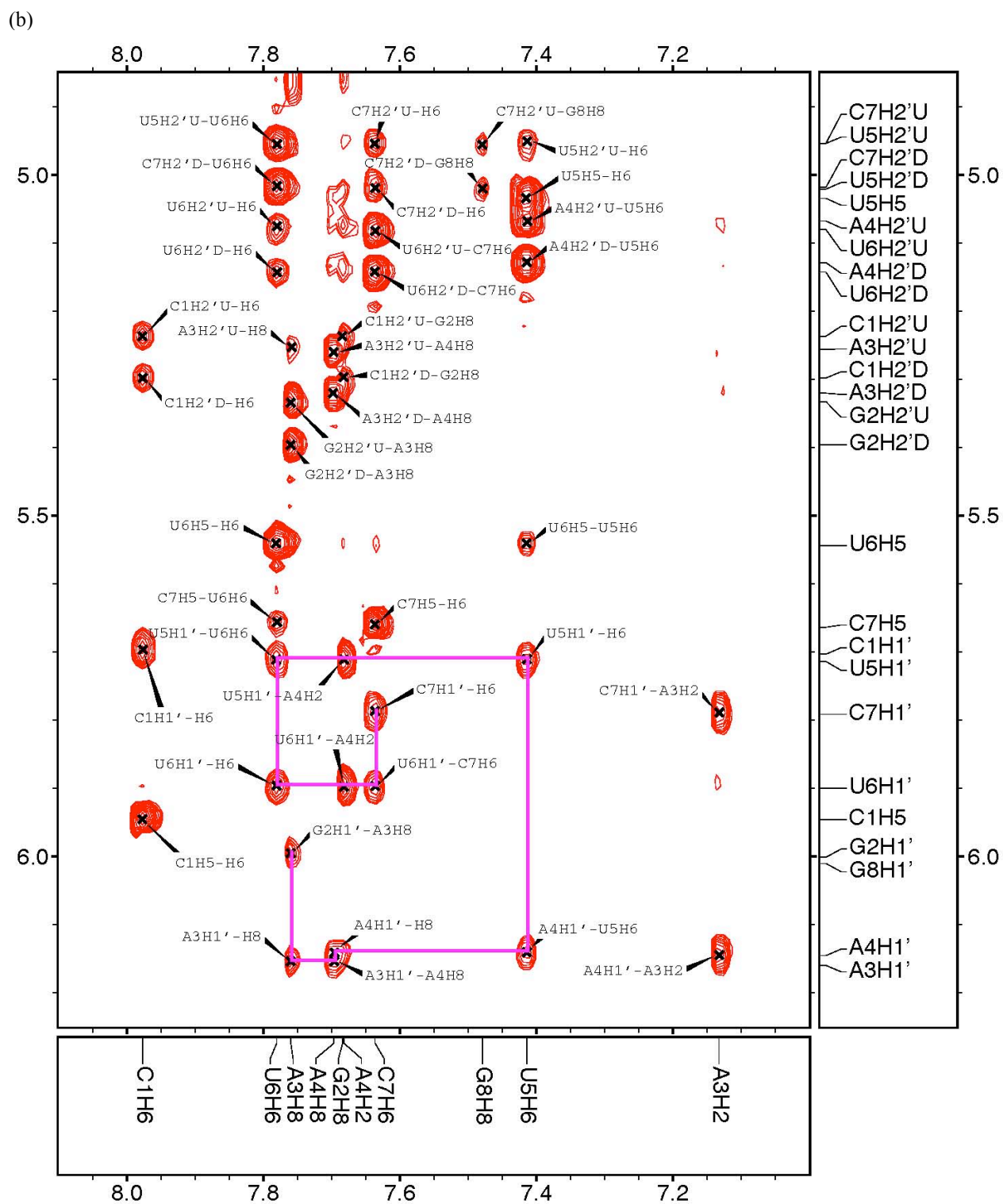


**Figure S2.** Expansion of the NOESY spectrum of (a)  $[r(\text{CGAAUUCG})]_2$  and (b)  $[f(\text{CGAAUUCG})]_2$  in buffered  $\text{D}_2\text{O}$  at 800 MHz, 298 K and a mixing time of 250 ms, showing NOE connectivities between H1' resonances of riboses and protons of nucleobases.

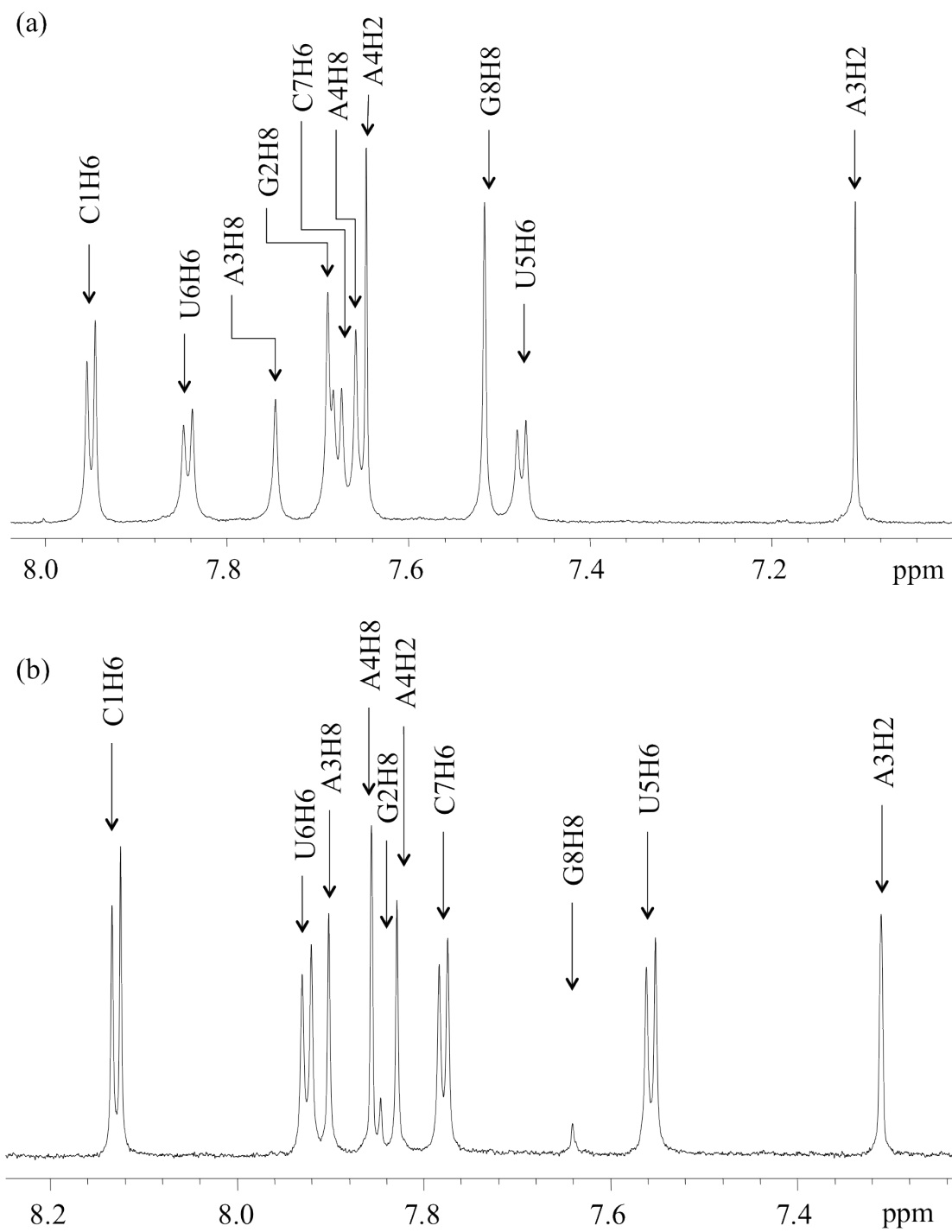


**Figure S3.** Low field region of  $^1\text{H}$ -NMR spectrum of (a)  $[\text{r}(\text{CGAAUUCG})]_2$  at 298 K and (b)  $[\text{f}(\text{CGAAUUCG})]_2$  at 313 K in phosphate-buffered  $\text{D}_2\text{O}$  at 800 MHz. Resonances of individual protons are labeled.

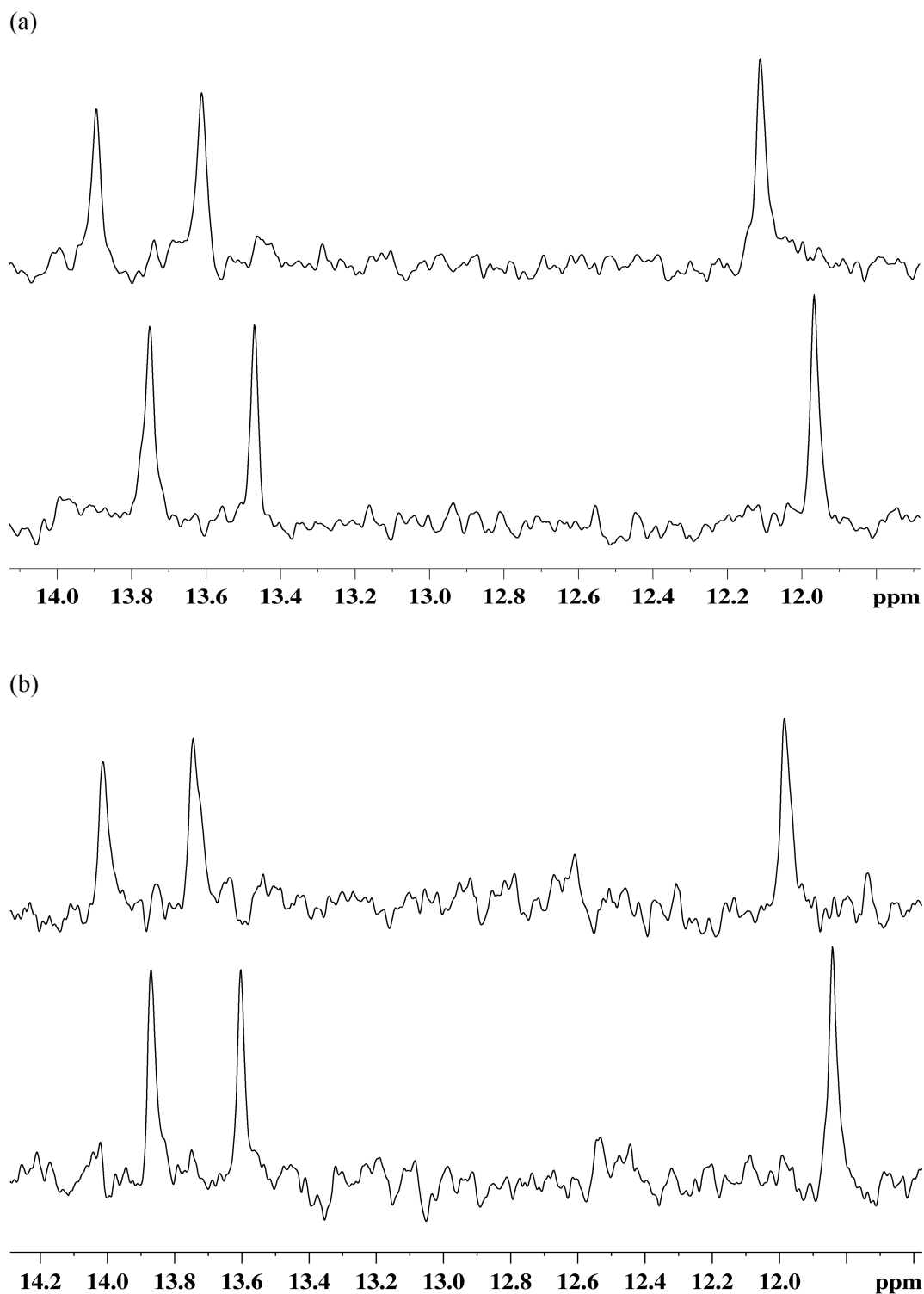


**Figure S4.** One-dimensional  $^{15}\text{N}$ -coupled  $^1\text{H}$  IPAP spectra in the imino region of (a) 5'-[r(CGAAUUCG)]<sub>2</sub> and (b) [f(CGAAUUCG)]<sub>2</sub> in 10% D<sub>2</sub>O/H<sub>2</sub>O at 5°C. The spectra at the top in (a) and (b) were obtained from adding the IP and AP spectra, whereas the lower spectra were obtained by subtraction, IP - AP.

**Table S1.** Deuterium isotope effect (DIE) measurements for RNA and 2'-F RNA<sup>a</sup>

Base Pair	RNA ( $\delta^{13}\text{C}2\{\text{H}3\}$ ) <sup>b</sup>	$\delta_{\text{H}3}$ (RNA)	2'-F RNA ( $\delta^{13}\text{C}2\{\text{H}3\}$ ) <sup>b</sup>	$\delta_{\text{H}3}$ (2'-F RNA)
<b>A3:U14</b>	-55.3±0.6	7.17	-63.6±0.1	7.15
<b>A4:U13</b>	-58.1±0.5	7.70	-62.8±0.2	7.70

<sup>a</sup> Units of  ${}^n\Delta A = \delta_A\{\text{H}3\} - \delta_A\{\text{H}3\}$  are in ppb, and units of  $\delta_{\text{H}3}$  are in ppm. <sup>b</sup> Shown here are values from two separate data sets.

## 2. UV thermal melting experiments

Melting of each oligonucleotide hairpin (16 mM) was performed in 10 mM sodium cacodylate (pH = 7.4), 0.1 mM EDTA, and 300 mM NaCl in the presence of 0, 5, 10, 15, and 20 % weight/volume of either ethylene glycol or acetamide (**Table 1**). Absorbance vs. temperature profiles were measured at 280 nm on a Shimadzu 800 UV-Visible spectrometer equipped with an eight-position Peltier temperature controller. The temperature was increased at 0.5 °C per minute. The melting temperatures were obtained using the Shimadzu LabSolution TmAnalysis software. The experimental absorbance vs. temperature curves were converted into a fraction of strands remaining hybridized ( $\alpha$ ) vs. temperature curves by fitting the melting profile to a two-state transition model, with linearly sloping lower and upper base lines. The melting temperatures ( $T_m$ , **Table 1**, column 2) were obtained directly from the temperature at  $\alpha = 0.5$ . The final  $T_m$  was an approximation of usually five to eight measurements.

The thermodynamic parameters ( $\Delta H$ ,  $\Delta S$  and  $\Delta G$ ) were obtained by van't Hoff analysis of melting curves using Varian Cary software (**Table 1**, columns 4-6). In addition, the enthalpy of the melting was determined from the width at the half-height of differentiated melting curves (**Table 1**, column 3). The fraction of strands remaining hybridized ( $\alpha$ ) vs. temperature curves were converted into differentiated melting curves [ $\delta\alpha/\delta(T_m^{-1})$  vs.  $T_m$ ] using Varian Cary software. The width of the differentiated melting curve at the half-height is inversely proportional to the van't Hoff transition enthalpy; for a monomolecular transition  $\Delta H = 7.0/(T_1^{-1} - T_2^{-1})$  where  $T_1$  is the lower temperature and  $T_2$  is the upper temperature (both in K) at one-half of [ $\delta\alpha/\delta(T_m^{-1})$ ].<sup>[1]</sup>

Osmotic stress experiments were performed as described in previous publications.<sup>[2]</sup> A detailed experimental manual has been also published.<sup>[3]</sup>

---

[<sup>1</sup>] K. J. Breslauer, *Methods Enzymol.* **1995**, 259, 221-242.

[<sup>2</sup>] (a) E. Rozners, J. Moulder, *Nucleic Acids Res.* **2004**, 32, 248-254. (b) P. S. Pallan, E. M. Greene, P. A. Jicman, R. K. Pandey, M. Manoharan, E. Rozners, M. Egli, *Nucleic Acids Res.* **2011**, 39, 3482–3495.

[<sup>3</sup>] E. Rozners, *Curr. Protoc. Nucleic Acid Chem.* **2010**, 7.14.1-7.4.13.

**Table S2.** Experimental  $t_m$  and thermodynamic data for melting of r[CGGUUUCGC]

Trial #	0%	5%	10%	15%	20%	T1	T2	$-\Delta H$ (cal/mol) $\delta\alpha/\delta T_m$	Van't Hoff - $\Delta H$ (kcal/mol)	Van't Hoff $-\Delta S$ (kcal/mol*K)	$\Delta G(37^\circ\text{C})$ (kcal/mo)
<b>Ethylene Glycol at 280nm</b>											
	52.5	51.7	50.5	49.9	49.0	39.34	66.58	27256	29.99	0.09193	-1.5
	51.5	51.6	50.2	50.1	48.7	38.73	64.85	28225	31.72	0.09772	-1.4
	51	51.9	50.3	50.0	48.3	38.17	64.01	28408	31.87	0.09832	-1.4
	52.7	51.1	50.3	48.3	48.4	38.88	65.26	27994	30.91	0.09497	-1.5
	52.1	51.4	50.5	49.8	48.6	41.07	69.05	26876	31.02	0.09449	-1.7
	51.6	50.9	50.2	49.2	48.2	38.81	64.95	28219	30.18	0.09275	-1.4
		51.9	50.3	49.4	47.3						
		51.8	50.5	49.9	48.8						
		52.6	50.0	49.0	48.9						
			50.5		48.5						
			50.8		48.7						
Average	51.9	<b>51.7</b>	<b>50.4</b>	<b>49.5</b>	<b>48.5</b>	39.2	65.8	27829.5	30.9	0.09503	-1.5
Standard Deviation	0.6	<b>0.5</b>	<b>0.2</b>	<b>0.6</b>	<b>0.5</b>	1.0	1.8	617.7	0.8	0.0025754	0.122359
<b>Acetamide at 280nm</b>											
		49.8	48.2	46.3	45.0						
		49.7	48.0	46.5	44.8						
		49.7	48.3	46.5	44.8						
		49.4	48.7	46	44.4						
		49.4	48.5	46.3	44.6						
		49.5	48.2	46.9	44.8						
		50.2	47.5	46.8	44.8						
		50.4	48.1	46.4	44.4						
		50.4		47	44.6						

		49.8								
Average		49.8	48.2	46.5	44.7					
Standard Deviation		0.4	0.4	0.3	0.2					

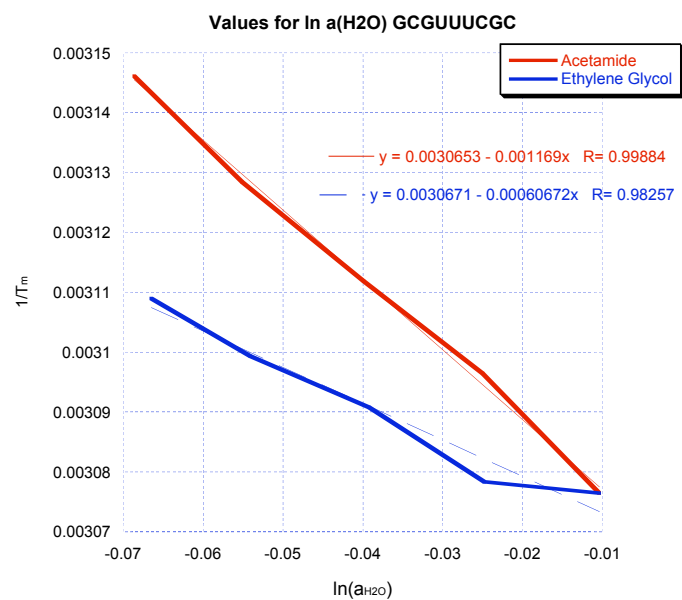


**Figure S5.** Plot of the inverse of the melting temperature versus the natural log of the water activity for both acetamide and ethylene glycol.

**Table S3.** Experimental  $t_m$  and thermodynamic data for melting of r(GCGUUUCGCA)

Trial #	0%	5%	10%	15%	20%	T1	T2	$\Delta H$ (cal/mol) $\delta\alpha/\delta T_m$	Van't Hoff $\Delta H$ (kcal/mol)	Van't Hoff $\Delta S$ (eu)	$\Delta G(37^\circ\text{C})$ (kcal/mol)
<b>Ethylene Glycol at 280nm</b>											
	64.1	63	61.3	56.7	55.5	53.1	76.9	33514	33.45	0.09905	-2.7
	63.4	62.6	61.0	57.2	55.9	52.8	76.4	33732	34.4	0.1	-2.8
	63.6	62.3	60.6	57.7	56.7	53.25	77.57	32920	33.93	0.1004	-2.8
	63	62.4	61.5	57.9	55.3	52.39	75.69	34087	33.69	0.1001	-2.7
	63.7	62.9	61.1	57.5	55.6	54.57	76.26	36923	37.56	0.1106	-3.3
	63.3	62.1	61.2	57.2	55.1	52.68	75.97	34159	34.1	0.1012	-2.7
	63.3				55.3	52.2	75.55	33980	34.09	0.1013	-2.7
						52.3	75.34	34427	33.84	0.1004	-2.7
						52.28	77.1	32118	36.34	0.1076	-3.0
						53.83	75.96	36076	36.58	0.1085	-2.9
						53.73	77.72	33436	36.57	0.108	-3.1
						53.14	75.8	35141	38.03	0.1127	-3.1
						52.72	75.75	34527	34.93	0.1034	-2.9
Average	63.5	<b>62.6</b>	<b>61.1</b>	<b>57.4</b>	<b>55.6</b>	53.0	76.3	34233.9	35.2	0.10426	-2.87396
Standard Deviation	0.4	<b>0.4</b>	<b>0.3</b>	<b>0.4</b>	<b>0.5</b>	0.7	0.8	1267.2	1.6	0.00459	0.19014
<b>Acetamide at 280nm</b>											
		61.1	57.4	55.7	52.9						
		60.1	57.5	55.2	53.4						
		61.7	58.0	55.0	52.8						
		61.4	57.4	55.6	53.2						
		60.2	57.2	55.3	52.0						
		61.1	57.6	55.1	52.5						
		60.9	58.3	55.1	52.3						

		60.4	57.6	56.2							
		61.0	57.9	56.2							
		60.9	58.0	55.6							
		60.3	58.2	56.2							
		60.1		55.8							
		60.7		55.8							
		60.2		56.0							
		59.9		56.3							
				55.7							
<b>Average</b>		<b>60.7</b>	<b>57.7</b>	<b>55.7</b>	<b>52.7</b>						
<b>Standard Deviation</b>		<b>0.5</b>	<b>0.4</b>	<b>0.4</b>	<b>0.5</b>						

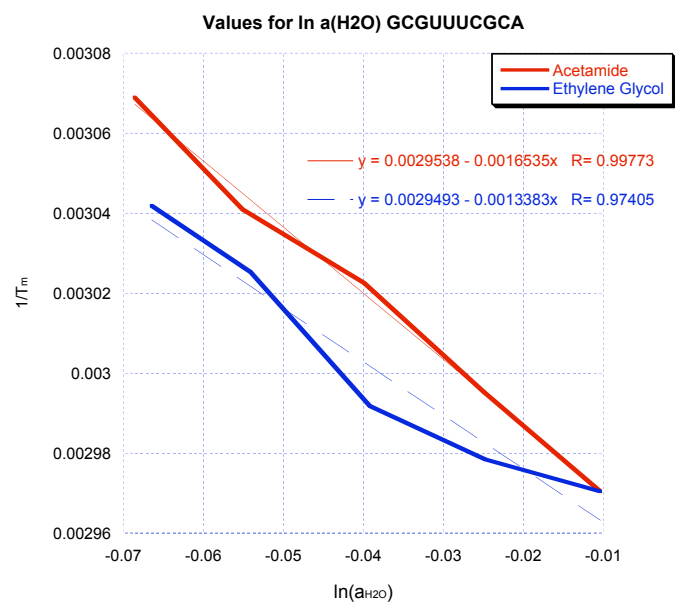


**Figure S6.** Plot of the inverse of the melting temperature versus the natural log of the water activity for both acetamide and ethylene glycol.

**Table S4.** Experimental  $t_m$  and thermodynamic data for melting of r(GCGUUUCGCAA)

Trial #	0%	5%	10%	15%	20%	T1	T2	$\Delta H$ (cal/mol) $\delta\alpha/\delta T_m$	Van't Hoff $\Delta H$ (kcal/mol)	Van't Hoff $\Delta S$ (eu)	$\Delta G(37^\circ\text{C})$ (kcal/mol)
<b>Ethylene Glycol at 280nm</b>											
	67.7	65.9	63.9	62	60.8	57.7	80.6	35770	38.56	0.1127	-3.623
	67.4	65.2	64	62.4	60.8	56.7	79.8	35270	39.8	0.1	-3.633
	68.1	66.4	64	62.7	60.8	55.4	78.34	35208	34.43	0.1014	-2.996
	67.6	65.7	63.8	62.4	60.5	55.4	79.08	34179	34.44	0.1013	-3.037
	68.4	65	63.8		60.9	56.6	81.31	33082	35.7	0.1043	-3.367
	67.9	65.2	63.8		60.6	56.4	80.09	34367	37.27	0.1092	-3.418
		65	63.8		60.4	57.6	79.41	37393	39.62	0.116	-3.66
		66.4	63.6		60.7	56.5	79	36084	40.03	0.1174	-3.636
		65.8	64		60.7	57.6	78.68	38608	42.24	0.1238	-3.862
		65.7	63.2		60.5	56.9	78.66	37320	40.1	0.1177	-3.613
Average	67.9	<b>65.6</b>	<b>63.8</b>	<b>62.4</b>	<b>60.7</b>	56.7	79.5	35728.1	38.2	0.11205	-3.4845
Standard Deviation	0.4	<b>0.5</b>	<b>0.2</b>	<b>0.3</b>	<b>0.2</b>	0.8	0.9	1682.0	2.7	0.007699	0.281094
<b>Acetamide at 280nm</b>											
		65.7	61.4	58.8	55.8						
		65.2	61.7	59.1	55.5						
		64.5	61.9	59	54.7						
		65.6	61.8	59	55.1						
		64.6		59.4	55.6						
		64.3		59.3	55.7						
					55.2						
					55.0						
					54.7						

Average		65.0	61.7	59.1	55.3					
Standard Deviation		0.6	0.2	0.2	0.4					

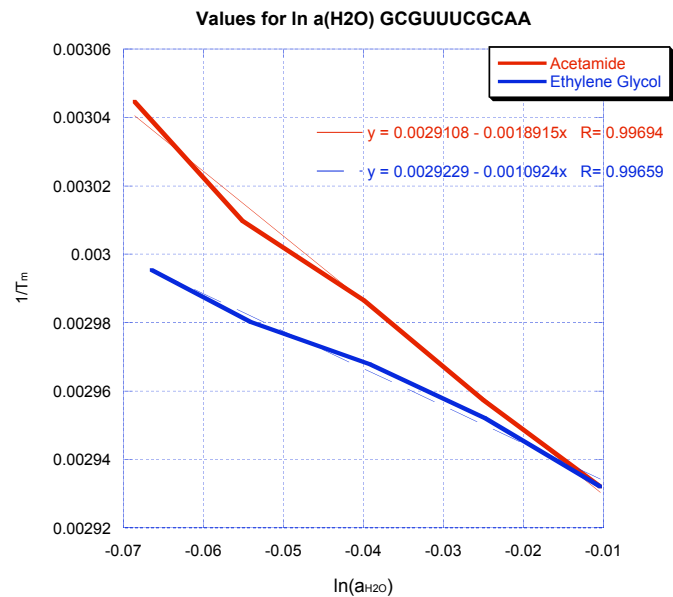


**Figure S7.** Plot of the inverse of the melting temperature versus the natural log of the water activity for both acetamide and ethylene glycol.

**Table S5.** Experimental  $t_m$  and thermodynamic data for melting of  $G_rCGUUUCG_Cr$

Trial #	0%	5%	10%	15%	20%	T1	T2	$\Delta H$ (cal/mol) $\delta\alpha/\delta T_m$	Van't Hoff $\Delta H$ (kcal/mol)	Van't Hoff $\Delta S$ (eu)	$\Delta G(37^\circ C)$ (kcal/mol)
<b>Ethylene Glycol at 280nm</b>											
	57.3	56.4	55.6	54	53.9	42.94	72.22	26075.19	29.59	0.08929	-1.9101
	57.1	56.2	56.1	54.7	53.4	43.12	71.36	26983.48	30.46	0.09215	-1.8935
	57.6	56.6	55.9	54.8	53.6	43.25	69.7	28682.5	31.17	0.09444	-1.8936
	57.6	56	55.4	55.1	52.9	43.55	72.14	26749.86	28.84	0.08711	-1.8359
	57.5	56.7	55.4	54.9	52.9	43.23	72.97	25751.27	29.65	0.08937	-1.9453
	57	55.8		54.3	53.8	42.32	73.31	24665.68	27.09	0.08153	-1.8157
		56.7		54.1	53.1						
		56		54.9	53.4						
				54.6							
Average	57.4	<b>56.3</b>	<b>55.7</b>	<b>54.6</b>	<b>53.4</b>	43.1	72.0	26484.7	29.5	0.088982	-1.88235
Standard Deviation	0.3	<b>0.4</b>	<b>0.3</b>	<b>0.4</b>	<b>0.4</b>	0.4	1.3	1353.8	1.4	0.004452	0.048132
<b>Acetamide at 280nm</b>											
		55.7	53.8	51.9	50.7						
		56.0	53.6	52.2	50.3						
		55.8	52.9	52.0	51.1						
		56.1	53.7		49.8						
		56.7									
Average		<b>56.1</b>	<b>53.5</b>	<b>52.0</b>	<b>50.5</b>						
Standard Deviation		<b>0.4</b>	<b>0.4</b>	<b>0.2</b>	<b>0.6</b>						

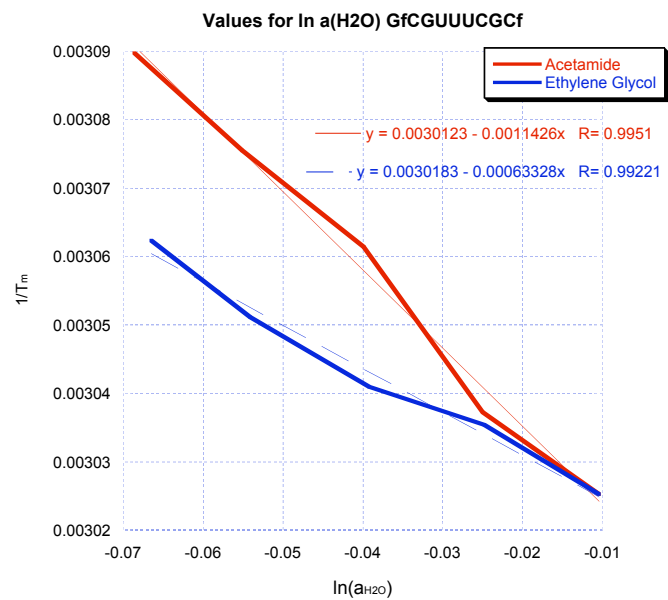


**Figure S8.** Plot of the inverse of the melting temperature versus the natural log of the water activity for both acetamide and ethylene glycol.

**Table S6.** Experimental  $t_m$  and thermodynamic data for melting of  $G_rCGUUUCGC_rA_f$

Trial #	0%	5%	10%	15%	20%	T1	T2	$\Delta H$ (cal/mol) $\delta\alpha/\delta T_m$	Van't Hoff $\Delta H$ (kcal/mol)	Van't Hoff $\Delta S$ (eu)	$\Delta G(37^\circ C)$ (kcal/mol)
<b>Ethylene Glycol at 280nm</b>											
	75	72.6	69.2	69.3	68.4	62.53	87.06	34475.19	37.64	0.1082	-4.098
	74.6	72.7	70.2	69.9	68.7	60.79	84.11	35780.37	39.75	0.1151	-4.069
	74.5	72.4	69.8	68.7	67.9	62.03	87.1	33686.08	37.16	0.1069	-4.021
	73.3	72.5	69.4	69.2	67.6	61.92	86.34	34498.41	37.38	0.1076	-4.024
	74	72.1	69.7	69.5	67.5	61.81	85.24	35834.24	37.64	0.1086	-3.974
	74.5	71.1	69.6	69	68	63.92	84.02	41891.06	39.74	0.1144	-4.276
	74.5	71.7	70.8	68.7	67.1						
		71.6	70.6	68.6	67.2						
		72.3	70.1	68.7	67						
		71.3	69.9	68.1	67.1						
		72		68.8	67.3						
		72.5		68.6	67.3						
		71.5		69	67.4						
				69.2	67.7						
Average	74.3	<b>72.0</b>	<b>69.9</b>	<b>69.0</b>	<b>67.6</b>	62.2	85.6	36027.6	38.2	0.110133	-4.077
Standard Deviation	0.5	<b>0.5</b>	<b>0.5</b>	<b>0.5</b>	<b>0.5</b>	1.0	1.4	2990.3	1.2	0.003629	0.106452
<b>Acetamide at 280nm</b>											
		72.0	67.9	66.0	64.6						
		70.9	67.7	65.5	63.7						
		71.8	67.5	65.2	63.9						
		70.0	67.8	66.3	63.7						

		69.9	68.2	66.0	64.2						
		70.0	67.4	65.3	64.0						
		71.7	68.5	65.8	63.9						
		70.6	67.9	65.8	63.8						
		70.3	67.4	66.1	64.1						
		70.0		66.8	63.4						
		71.5		65.0	63.7						
		69.9		65.4	63.5						
Average		<b>70.7</b>	<b>67.8</b>	<b>65.8</b>	<b>63.9</b>						
Standard Deviation		<b>0.8</b>	<b>0.4</b>	<b>0.5</b>	<b>0.3</b>						

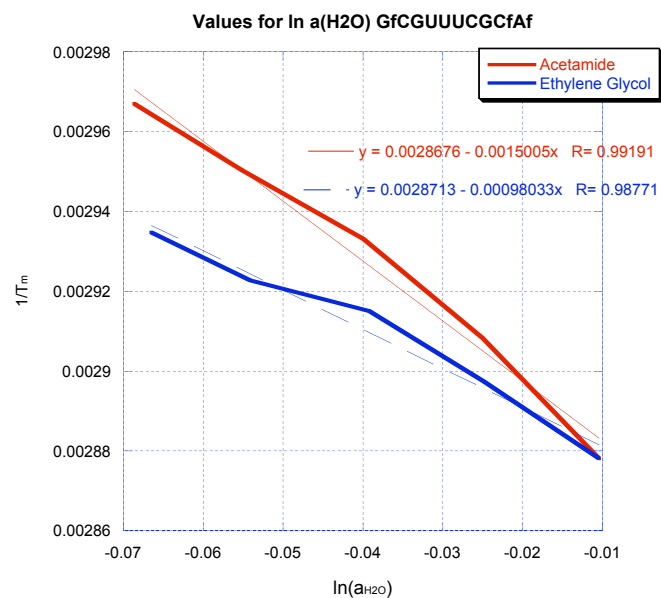


**Figure S9.** Plot of the inverse of the melting temperature versus the natural log of the water activity for both acetamide and ethylene glycol.

**Table S7.** Experimental  $t_m$  and thermodynamic data for melting of G<sub>r</sub>CGUUUCGC<sub>r</sub>A<sub>r</sub>A<sub>r</sub>

Trial #	0%	5%	10%	15%	20%	T1	T2	$\Delta H$ (cal/mol) $\delta\alpha/\delta T_m$	Van't Hoff $\Delta H$ (kcal/mol)	Van't Hoff $\Delta S$ (eu)	$\Delta G(37^\circ C)$ (kcal/mol)
<b>Ethylene Glycol at 280nm</b>											
	77.2	74.9	72.7	71.3	69.3	65.69	88.91	36952.07	38.59	0.1102	-4.428
	77	73.9	72.1	71.6	69.3	64.89	89.02	35485.31	39.05	0.1117	-4.423
	76.8	74.7	72.5	71	69.3	64.5	88.16	36062.57	39.83	0.1139	-4.521
	76.5	74.5	71.9	71.1	69.8	67.02	89.94	37689.7	40.85	0.1161	-4.859
	77.4	74	72.6	71.2	68.8	64.33	87.69	36459.8	39.69	0.1138	-4.412
	77.2	74.9	72.4	71	68.8	65.73	90.34	35006.87	36.95	0.1053	-4.307
	77.3	73.8	72.2	71.6	68.9						
		74.7	73	71.1							
		75	73	71.4							
		74.0	73.2	71.3							
		74.9	72.7	70.6							
				70.0							
Average	77.1	<b>74.5</b>	<b>72.6</b>	<b>71.1</b>	<b>69.2</b>	65.4	89.0	36276.1	39.2	0.111833	-4.49167
Standard Deviation	0.3	<b>0.5</b>	<b>0.4</b>	<b>0.4</b>	<b>0.4</b>	1.0	1.0	976.8	1.3	0.003787	0.19236
<b>Acetamide at 280nm</b>											
		74.3	70.6	69.2	66.0						
		73.7	71.2	68.4	66.1						
		73.5	72.0	68.1	65.4						
		73.3	70.9	68.7	66.9						
		73.8	71.0	69.5	65.7						
		74.4	70.5	69.4							
		72.7	70.8								

		73.5								
Average		<b>73.7</b>	<b>71.0</b>	<b>68.9</b>	<b>66.0</b>					
Standard Deviation		<b>0.5</b>	<b>0.5</b>	<b>0.6</b>	<b>0.6</b>					

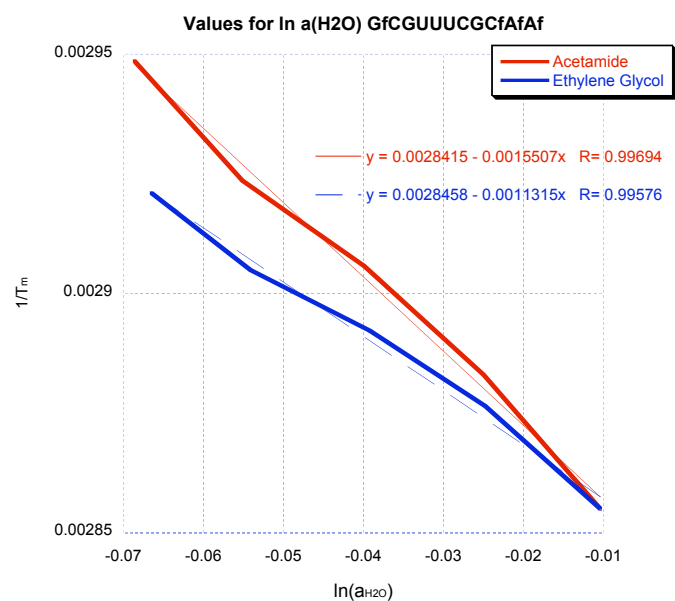


**Figure S10.** Plot of the inverse of the melting temperature versus the natural log of the water activity for both acetamide and ethylene glycol.

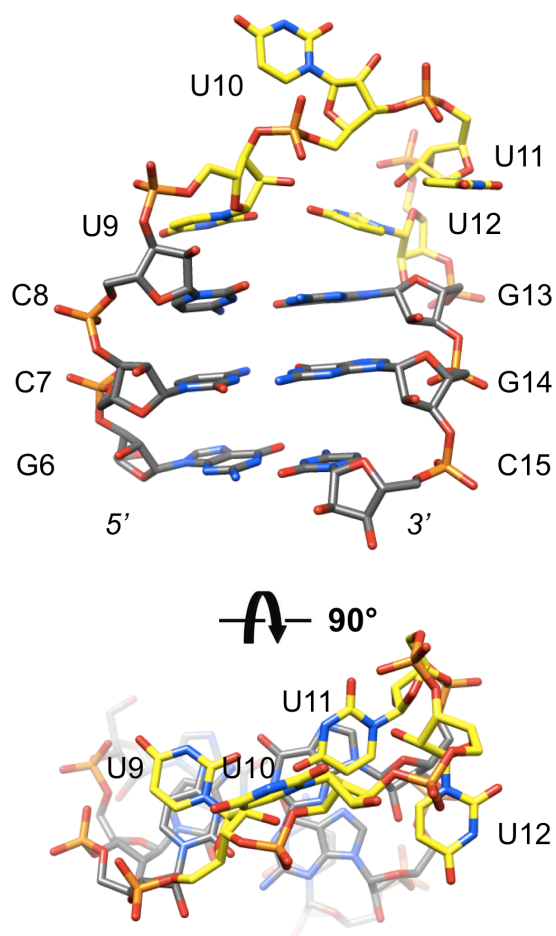


**Figure S11.** NMR solution structure of a portion of the U2 snRNA stem I from *S. cerevisiae* (PDB ID 2o33)<sup>[4]</sup> viewed into the minor groove (top) and rotated around the horizontal by 90 degrees (bottom). Only the (GCC):(GGC) stem and the U4 loop are depicted, with carbon atoms colored in gray and yellow, respectively. The two projections illustrate the absence of stacking among loop uracils and very limited stacking between U9 and C8 and between U12 and G13. Similarly, no hydrogen bonds are established between nucleobase moieties from loop residues.

[4] D. G. Sashital, V. Venditti, C.G. Angers, G. Cornilescu, S. E. Butcher, *RNA* **2007**, *13*, 328–338.